

LA-UR-19-26111 (Accepted Manuscript)

A finite scale model for shock structure

Margolin, Len G.
Plesko, Catherine Suzanne
Reisner, Jon Michael

Provided by the author(s) and the Los Alamos National Laboratory (2020-01-03).

To be published in: Physica D: Nonlinear Phenomena

DOI to publisher's version: 10.1016/j.physd.2019.132308

Permalink to record: <http://permalink.lanl.gov/object/view?what=info:lanl-repo/lareport/LA-UR-19-26111>

Disclaimer:

Los Alamos National Laboratory, an affirmative action/equal opportunity employer, is operated by Triad National Security, LLC for the National Nuclear Security Administration of U.S. Department of Energy under contract 89233218CNA000001. By approving this article, the publisher recognizes that the U.S. Government retains nonexclusive, royalty-free license to publish or reproduce the published form of this contribution, or to allow others to do so, for U.S. Government purposes. Los Alamos National Laboratory requests that the publisher identify this article as work performed under the auspices of the U.S. Department of Energy. Los Alamos National Laboratory strongly supports academic freedom and a researcher's right to publish; as an institution, however, the Laboratory does not endorse the viewpoint of a publication or guarantee its technical correctness.

Journal Pre-proof

A finite scale model for shock structure

L.G. Margolin, C.S. Plesko, J.M. Reisner

PII: S0167-2789(19)30401-4

DOI: <https://doi.org/10.1016/j.physd.2019.132308>

Reference: PHYSD 132308

To appear in: *Physica D*



Please cite this article as: L.G. Margolin, C.S. Plesko and J.M. Reisner, A finite scale model for shock structure, *Physica D* (2019), doi: <https://doi.org/10.1016/j.physd.2019.132308>.

This is a PDF file of an article that has undergone enhancements after acceptance, such as the addition of a cover page and metadata, and formatting for readability, but it is not yet the definitive version of record. This version will undergo additional copyediting, typesetting and review before it is published in its final form, but we are providing this version to give early visibility of the article. Please note that, during the production process, errors may be discovered which could affect the content, and all legal disclaimers that apply to the journal pertain.

© 2019 Published by Elsevier B.V.

A Finite Scale Model for Shock Structure

L.G. Margolin^a, C.S. Plesko^a, J.M. Reisner^a

^a*Computational Physics (XCP) Division, Los Alamos National Laboratory, MS F644, Los Alamos, NM 87545, len@lanl.gov*

Abstract

In this paper we explore the use of a finite scale model of fluid dynamics to predict the finite structure of a shock wave in a perfect gas. We begin by documenting the history and issues that have arisen when Navier–Stokes theory is applied to the shock structure problem, and continue by motivating the improvement that finite scale theory might provide from its representation of inviscid (anomalous) dissipation. Our primary results include the formulation of a traveling wave equation from finite scale theory, an analysis of the solutions of that equation as regards shock width and monotonicity properties, and an estimation of the critical parameter of the theory from experimental data.

Keywords:

Preamble

There is a close connection between turbulence and shock waves, both in the sense of physics and in the sense of numerical simulation. Physically, both are examples of high Reynolds number flows, meaning that the length scales of advection are much larger than the length scales of dissipation. Numerically, both are modeled by the Euler equations regularized by dissipation depending on the square of the computational cell size – i.e., subgrid scale models in turbulent flows [38] and artificial viscosity in shocks [46].

The simultaneous presence of turbulence and shocks in Richtmyer–Meshkov instability introduces both complexity and opportunity [53, 54]. David Youngs was the first to recognize and seize that opportunity. In a remarkable series of papers [48, 49, 50, 19, 51, 43, 52, 16] spanning more than 35 years, David exploited the ideas of implicit turbulence modeling and became one of the pioneers of the technique now termed implicit large eddy simulation or ILES [11]. David employed the nonoscillatory advection schemes of van Leer, which were first developed to enforce monotonicity and eliminate unphysical oscillations in numerical simulations of shock propagation [45]. He recognized that the dissipative properties of the van Leer scheme would selectively damp the shortest wavelength motions of a turbulent flow and so provide an effective *implicit* turbulence model.

A more rigorous rationale for ILES was offered in 2002 by Margolin & Rider [26]. That justification lay in deriving the equations that finite volumes of fluid obey and showing that those equations, termed the finite scale Navier–Stokes or FS (equations written out in section 3), are in fact the regularized Euler equations that are the basis of the numerical simulation of high Reynolds number flows as described above. However, the derivation makes no specific reference to simulation, to turbulence or shocks. That generality has led the authors here to speculate that FS might provide a theoretical model for shocks, which investigation is the subject of the present paper.

1. Introduction

“There is no cure for curiosity.” (Dorothy Parker)

In this paper, we will explore the *plausibility* of using finite scale theory to describe the continuum shock structure of a perfect gas. It is well known that the compressible Navier–Stokes equations predict spatial shock profiles, e.g., of density and velocity, that are too narrow and too asymmetric when compared to experiment [1, 37]. In our main result, we will develop analytic solutions based on the finite scale equations applied to shock waves. We will show that in comparison to the Navier–Stokes solutions, the finite-scale solutions exhibit the experimentally observed trends to wider shock profiles.

Finite scale theory was first developed as a model for turbulent flow, which is a high Reynolds number phenomenon. In particular, the finite scale equations contain *inviscid* dissipation, sometimes referred to as anomalous dissipation [7, 8]. Similarly, the interior of a shock is a region of high Reynolds number where the effects of anomalous dissipation can be expected to widen the predicted shock profile. Preliminary attempts to apply the finite scale theory to study shock structure [28, 15] have used truncated forms of the finite scale equations, neglecting the effects of heat conduction. In this paper we will consider the full finite scale equations, which include physical viscosity and heat conduction plus additional the finite-scale fluxes of momentum and energy. We will derive analytic solutions for shock structure and use those results to estimate the shock width and symmetry of the profile.

We remark that this paper does not constitute a complete theory; the finite scale equations, as the name implies, contain a length scale which in the case of shocks represents the point at which continuum theory fails. A theoretical estimate of that length scale needs to come from kinetic theory. Here, we will use experimental data to estimate that length scale.

The outline of this paper is as follows. In section 2 we discuss the history of shock structure theory and the discrepancies that exist between predictions based on Navier–Stokes theory and experimental measurement. In section 3, we introduce the finite scale equations for perfect gases and provide some motivation why they might provide a more accurate description of shock structure. In section 4, we formulate the traveling wave equations for shock waves and manipulate them into an ODE for the velocity. We discuss the role of the finite scale parameter (\mathcal{B}) and its relation to the microscale parameter of mean free path. In section 5, we show how to estimate this parameter from published

experimental data and then demonstrate the universality of the parameter for shocks of varying strengths (Mach numbers).

In section 6, we explore some properties of the finite scale profiles, using both theory and numerical solution to discuss solution properties such as monotonicity and lack of compactness, and to compare the profiles with those computed from Navier–Stokes theory. We conclude in section 7 with a summary of results and strategies for continuing our study of finite scale shock structure.

2. Shocks in Theory and in Nature

A shock is a wave that moves faster than the local speed of sound in a fluid. Although shocks are often idealized mathematically as being discontinuous, physical shocks measured in the laboratory have a finite width and permanent shape. The earliest attempts to build a theory of shock waves were hampered by the lack of recognition of the principle of conservation of energy. A history of those attempts in the 19th century can be found in the informative review by Salas [36]. Below we will review the more recent efforts to analytically model the shock profile and then summarize the experimental results of Schmidt [37] and of Alsmeyer [1].

2.1. Shocks in theory

The shock profile, i.e., the spatial dependence of density, velocity and internal energy and its characterization by the metric of the shock width, is a well-studied problem with an extensive literature; a recent survey can be found in [44]. What might be termed the Navier–Stokes phase of that literature began with the articles of Rayleigh [33] and Taylor [40], both in 1910, in which the general one-dimensional (1D) equation of motion for the Navier–Stokes shock profile was first derived; those authors, however, were only able to obtain solutions for either the special case of constant viscosity with no heat conduction or the other special case of constant heat conductivity with no viscosity. Becker’s 1922 publication [2] is usually cited for deriving a steady shock solution of the compressible Navier–Stokes equations containing both viscosity and heat conduction. However, Becker’s main purpose was to question the validity of Navier–Stokes for describing shocks. To understand the connection, we need to provide some additional context.

The Chapman–Enskog approximation, first published by Chapman (1916) and Enskog (1917) [6] derives the Navier–Stokes equations by perturbation expansion of the more fundamental Boltzmann equation. The expansion parameter is the Knudsen number, the dimensionless ratio of the molecular mean free path to a *macroscopic* length scale. At zeroth order that expansion leads to the Euler equations and at first order to Navier–Stokes. An important consequence of this derivation is the explicit dependence of the macroscopic transport parameters of viscosity and thermal conductivity on the microscopic mean free path. In the shock problem, the macroscopic length scale is the shock width. Thus, by virtue of his steady shock solution, Becker was able to estimate that

a shock was only about one or two mean free paths wide; this implies that the Knudsen number is not small and leads to Becker's main point, namely that Navier–Stokes theory should not be applicable within the shock profile. A succinct discussion of the Chapman–Enskog procedure can be found in [17].

Becker's paper received little attention for many years. In 1944, Thomas [42] pointed out that the Becker analysis had neglected the dependence of the viscosity and thermal conductivity on temperature, which qualitatively would be expected to widen the theoretical prediction of the shock width. That was followed in 1949 by the important paper of Morduchow & Libby [29] in which the effects of temperature dependence were quantitatively assessed (by quadrature); temperature dependence was shown to have some quantitative effect, but did not qualitatively negate Becker's criticism. We note that [29] is perhaps best known today for a peripheral result in which Morduchow & Libby evaluated the thermodynamic entropy and showed that it had a maximum within the shock profile. This surprising result, however, has been shown not to violate the second law of thermodynamics; see [25] for a discussion.

It would take more than thirty years after Becker for the experimental corroboration, but indeed detailed measurements show that the density profiles of physical shocks are typically twice as wide as Navier–Stokes theory predicts, and are more symmetric in shape [1, 37]. The results are nicely summarized in Fig. 10 of Schmidt's paper [37] which compares the inverse of the (normalized) shock width plotted against Mach number as predicted by Navier–Stokes theory (curve 1) and as measured experimentally (curve 3). Those results will play a primary role in our paper. Note that the experimental results show as clusters of points, indicating both the uncertainty of measurement and the natural stochasticity of the shock.

In 1968, Bird published calculations of shock structure based on direct simulation Monte Carlo (DSMC) solutions of the Boltzmann equation [4]. Those solutions are in excellent agreement with the data, both in terms of shock width and shape. Since the Navier–Stokes equations can be derived as an approximation of the Boltzmann equation, one might conclude that agreement with the experimental profiles might be improved by keeping higher-order terms in the Chapman–Enskog expansion. However, the next order of the expansion, i.e., the Burnett equations, does not provide any significant improvement in reproducing the measured data [10]. In section 3 of [17], Kremer writes

“The Knudsen number is related to the degree of rarefaction of a gas. When $Kn \ll 1$ the molecular collisions are very important, the distribution function is determined by the collision term of the Boltzmann equation and the gas is described by a continuum regime. Otherwise, when $Kn \gg 1$ molecular collisions become negligible, the distribution is determined via a collisionless Boltzmann equation.”

Kremer's quote would seem to imply that a continuum description is only possible when one is in a collision-dominated regime. However, another possibility exists in which *anomalous dissipation* is present in addition to the viscous dissipation due to collisions; see e.g., chapter 5 of [8]. In finite scale theory, this

additional dissipation results from spatial averaging of the (nonlinear) advective terms. We will expand on this in section 3.

Analytic approaches to modeling fluid shock structure as described above have been restricted to perfect gases¹, i.e., gases for which the thermodynamic pressure p is simply related to the density ρ and internal energy \mathcal{E} by the ideal gas law

$$p = (\gamma - 1)\rho\mathcal{E}.$$

Here $\gamma = c_p/c_v$ is the ratio of specific heats at constant pressure c_p and at constant volume c_v , both of which are assumed to be independent of temperature. However, computational studies are not so limited and have been applied to more general equations of state for gases and liquids. Detailed simulations of the Boltzmann equation allow one to isolate and evaluate the effects of nonequilibrium processes and stochasticity. Beyond the DSMC results described above, detailed studies of shock structure have been published using nonequilibrium molecular dynamics (NEMD) [13, 14], gas kinetic Bhanagar-Gross-Krook (BGK) approximation [5], and lattice Boltzmann (LB) techniques [39, 35]. Each of those computational techniques, NEMD, DSMC, BKG and LB, is particle-based and so preserves the stochasticity of solutions of the Boltzmann equation. Further, all of the studies referenced above support the basic conclusion that the Boltzmann equation contains sufficient physics to accurately describe the shock structure of a perfect gas.

2.2. Shocks in the laboratory

There are many papers that report the spatial dependence of the shock profile in gases; see e.g., [37] and [1] and the many references within. Among those papers that compare the laboratory measurements with theory, there is consensus that the Navier–Stokes equations do not accurately predict the width nor the shape of the measured profiles. Here, we summarize some relevant results of Schmidt [37] and Alsmeyer [1].

Both Schmidt and Alsmeyer provide detailed descriptions of the experimental procedure, identifying sources and estimating experimental error which *in toto* is asserted to be less than 5%. A larger source of uncertainty results from the stochastic nature of the flow. The clusters of ‘in principle’ identical measurements in Fig. 10 of Schmidt suggest an uncertainty of perhaps 10% due to stochasticity. Also, the faired curve in that figure based on the Mott–Smith theory [30] appears to lie slightly above most of the actual data points.

Despite those uncertainties, some main trends of the data seem clear.

- Figure 10 of Schmidt shows that Navier–Stokes estimates of the shock width are only about half the measured widths.
- Figure 5 of Schmidt shows that the “normalized profiles of density” are independent of shock strength (Mach number), except for a small departures near the foot of the shock.

¹Also sometimes termed polytropic or gamma-law gases.

- Figure 8 of Alsmeyer shows that the shock shape predicted by Navier–Stokes theory is more asymmetric than are the measurements. Both the normalized profiles and the measure of asymmetry are defined on page 369 of [37].

There is an important issue that precludes us from making direct comparison of finite scale predictions with the experimental data. The transport coefficients, e.g., the viscosity, μ , and the thermal conductivity with respect to the gradient of the internal energy, κ , depend on the temperature. The measured shock profiles, of course, reflect the effects of that temperature dependence. Although it is not stated explicitly, the theoretical Navier–Stokes calculations reported in both Schmidt and Alsmeyer also incorporate temperature dependence; cf. the caption of Figure 8 in Schmidt and the first sentence of page 502 in Alsmeyer. Our derivation and hence the solution found in section 4 do not take the temperature dependence into account.

For the Navier–Stokes equations, the effects of temperature dependence on the transport coefficients has been briefly investigated numerically; see e.g., figures 3 and 4 in [25] where it is shown that the temperature dependence broadens the foot of the shock and so increases the asymmetry of the shock profile.

3. Finite Scale Equations

We present a short history of finite scale theory, and then exhibit the finite scale equations (FS). The FS resemble Navier–Stokes equations but contain additional fluxes of momentum and energy that arise from the nonlinearity of advection. We will discuss the salient features that distinguish FS from the compressible Navier–Stokes equations below.

The story of finite scale Navier–Stokes (FS) begins with a numerical technique termed implicit large eddy simulation (ILES) employed for simulating turbulent flows. In essence, the technique consists of employing one of many nonoscillatory finite volume (NFV) algorithms and allowing the numerical dissipation to replace the physical dissipation that is unresolved in the simulation. The concept was first proposed by Jay Boris [31] to simulate problems in plasma turbulence. Subsequently and independently, ILES was used in [19] to model the growth of fluid instabilities, in [32] to model astrophysical turbulence and in [27] to model atmospheric boundary layers. Each of these applications used a different NFV algorithm while achieving physically relevant results.

In the period before the year 2000, the use of ILES was controversial, sometimes disparagingly termed *no model LES*. Despite the quality of the aforementioned results, the lack of a physical justification impeded its general acceptance. In 2002, Margolin & Rider [26] provided a rationale for ILES. The main result of that paper answered the following question:

“If the field variables, e.g., density, velocity, energy, of every point of a fluid in a finite volume is governed by the Navier–Stokes equations, what equations govern the volume averages of those field variables?”

The pertinent equations derived in [26] are in fact the FS and are exhibited below. Further, it was demonstrated that computer programs formulated to solve high Reynolds number flows (in both the Eulerian and the Lagrangian frameworks) solve a form of the FS in the sense of the *modified equation* [12]. Thus, the rationale for ILES is that discretized equations of the computer codes are actually solving the equations that govern the evolution of the volume-averaged field variables in the computational cells. That justification was shortly followed by a book [11] in which many of the pioneers contributed a variety of examples demonstrating the accuracy and generality of ILES. Now ILES is widely accepted and used by the turbulence modeling community. A more complete description of the inception of ILES by Jay Boris can be found in chapter 1 in [11], and of the subsequent early history of ILES can be found in section 4 of [21].

Although the FS were first derived as a PDE model for turbulent simulations, that derivation makes no reference either to turbulence or to simulation. The derivation in [26] combines a renormalization of the Navier–Stokes equations with induction. Expanded discussions of the derivations can be found in [20, 21, 24, 23]. In [20], it was suggested that the FS might provide the appropriate *theoretical* basis for more general descriptions of high Reynolds number flows, in particular for flows with shocks. First explorations of that idea appear in [28] and in [15] where traveling wave solutions of two forms of the adiabatic FS equation are presented. Here, *adiabatic* implies that the fluxes of heat conduction, both Fourier and finite scale, are ignored. In our main results of section 4 we will show traveling wave solutions for the full FS.

Below, we write the finite scale Navier–Stokes equations for a compressible perfect gas in one spatial dimension [20]. We use internal energy rather than temperature, but note that for a perfect gas the former is proportional to the latter with the constant of proportionality being c_v which is assumed to be constant.

$$\frac{\partial \rho}{\partial t} + \frac{\partial \rho u}{\partial x} = 0 \quad (1)$$

$$\frac{\partial \rho u}{\partial t} + \frac{\partial}{\partial x} (\rho u^2 + P) \quad (2)$$

$$\frac{\partial}{\partial t} \left(\mathcal{E} + \frac{1}{2} \rho u^2 \right) + \frac{\partial}{\partial x} \left(\mathcal{E} u + \frac{1}{2} \rho u^3 + P u + Q \right) = 0 \quad (3)$$

$$P = (\gamma - 1) \rho \mathcal{E} - \mu \frac{\partial u}{\partial x} + A \rho \left(\frac{\partial u}{\partial x} \right)^2 \quad (4)$$

$$Q = -\kappa \frac{\partial \mathcal{E}}{\partial x} + \gamma A \rho \left(\frac{\partial u}{\partial x} \right) \left(\frac{\partial \mathcal{E}}{\partial x} \right) \quad (5)$$

Here, ρ, u , and \mathcal{E} have their usual meanings of density, material velocity and internal energy. The total pressure P in eq. (4) contains three contributions. The first term is the ideal gas law, which is a good approximation to the behavior of many gases. The second term is Newton’s law of viscosity and the third term

represent the finite scale contribution. The heat flux Q in eq. (5) consists of Fourier's law plus a finite scale contribution.

The transport coefficient, μ , is the longitudinal coefficient of viscosity and κ is the thermal conductivity with respect to the gradient of the internal energy. Note that both μ and κ are dynamic (or absolute) coefficients, i.e., both have the units of $(M/L^3)(L^2/T) = M/(LT)$. The final terms of eqs. (4) and (5) are proportional to the density. The constant parameter A has the dimension of length squared – in the case of numerical simulation

$$A = \frac{1}{3} \left(\frac{\Delta x}{2} \right)^2 \quad (6)$$

where Δx is the computational cell size. More generally, Δx is to be interpreted as a length scale representing an *observer*; see [21]. Terms proportional to A in eqs. (4) and (5) are the *finite scale* fluxes of momentum and energy. Those fluxes, representing the anomalous dissipation, arise from lack of commutativity of the averaging process with multiplication; i.e., the average of the product is not the product of the averages. We mention for completeness that the velocity u that appears is the Favre-averaged velocity and similarly the internal energy \mathcal{E} is the Favre-averaged internal energy, although those distinctions play no role in this paper.

We note two aspects of the equations that do play a surprisingly important role in this paper. First, the finite scale fluxes are proportional to physical density whereas the physical fluxes of momentum and energy are not. Second, there is an “extra” factor of γ that arises in the finite scale flux of energy. The origin of that factor is discussed in section 4 of [20].

We draw attention to the similarity between the finite scale flux of momentum and the Reynolds stress terms introduced to represent the effects of velocity fluctuations in turbulent flow [41]; that analogy becomes evident when the association is made between the velocity fluctuations u' and $\frac{\partial u}{\partial x} \Delta x$. The connection between the finite scale fluxes and subgrid scale models of turbulence is explored in more detail in [24]. The finite scale fluxes are the spatially averaged correlation of fluctuations and so introduce the long range effects of stochasticity into the equations. This is practically demonstrated in Fig. 4 where the velocity profile of the FS shock is shown to be significantly wider than that of the Navier–Stokes shock.

4. Traveling Wave Solutions

We will look for traveling wave solutions of the finite scale equations. Our analysis is closely related to Becker's derivation of steady state solutions of the Navier–Stokes equations for shock wave structure; like Becker, we will assume a particular Prandtl number, which results in the conservation of enthalpy through the shock profile. The relation of traveling wave solutions to the steady state analysis of Becker [2] and the later important contribution of Morduchow & Libby [29] are discussed in detail in [25].

To derive the traveling wave equations for a shock, we assume that all the field variables depend on space and time through the similarity variable $y \equiv x - vt$, where the constant v will turn out to be the velocity of the shock. We model a shock moving to the right into a gamma law gas at rest whose density is ρ_o and whose internal energy is \mathcal{E}_o . The shock is driven by a “piston” with velocity u_p . Thus the asymptotic conditions are:

$$\rho \rightarrow \rho_o \quad ; \quad u \rightarrow 0 \quad ; \quad \mathcal{E} \rightarrow \mathcal{E}_o \quad \text{as } y \rightarrow +\infty$$

$$u \rightarrow u_p \quad ; \quad \frac{du}{dy}, \frac{d\rho}{dy}, \frac{d\mathcal{E}}{dy} \rightarrow 0 \quad \text{as } y \rightarrow -\infty$$

Applying the similarity assumption to eqs. (1)–(5) and integrating the resulting ODEs from a point y to $+\infty$ then results in:

$$\rho(v - u) = \rho_o v \quad (7)$$

$$u\rho(v - u) - (\gamma - 1)\rho\mathcal{E} + \mu \frac{du}{dy} - A\rho \left(\frac{du}{dy}\right)^2 = -p_o = -(\gamma - 1)\rho_o\mathcal{E}_o \quad (8)$$

$$\begin{aligned} \rho\mathcal{E}(v - u) + \frac{1}{2}\rho u^2(v - u) - (\gamma - 1)\rho\mathcal{E}u + \mu u \frac{du}{dy} - Au\rho \left(\frac{du}{dy}\right)^2 \\ + \kappa \frac{d\mathcal{E}}{dy} - A\gamma\rho \frac{du}{dy} \frac{d\mathcal{E}}{dy} = v\mathcal{E}_o\rho \end{aligned} \quad (9)$$

The shock speed v is determined by conservation and is related to the piston speed by:

$$v^2 - \frac{\gamma + 1}{2} u_p v - c_o^2 = 0. \quad (10)$$

where c_o is the sound speed in the stationary (downstream) portion of the fluid

$$c_o \equiv \sqrt{\gamma(\gamma - 1)\mathcal{E}_o}. \quad (11)$$

We define the Mach number \mathcal{M}

$$\mathcal{M} \equiv \frac{v}{c_o}. \quad (12)$$

Then the shock velocity, the piston velocity and Mach number are related by:

$$u_p = \frac{2v}{(\gamma + 1)} \left(1 - \frac{1}{\mathcal{M}^2}\right). \quad (13)$$

Momentum

Eliminating density from the momentum equation leads to:

$$(\gamma - 1)\mathcal{E} = u(v - u) + \frac{\mu}{\rho_o} \left(\frac{v - u}{v}\right) \frac{du}{dy} - A \left(\frac{du}{dy}\right)^2 + (\gamma - 1)\mathcal{E}_o \left(1 - \frac{u}{v}\right) \quad (14)$$

Energy

Next, multiply the momentum equation by $-v$ and add to the energy equation.

$$\begin{aligned} \gamma\rho\mathcal{E}(v-u) + \rho u(v-u)\left(\frac{1}{2}u-v\right) + \mu(u-v)\frac{du}{dy} - \rho A(u-v)\left(\frac{du}{dy}\right)^2 \\ + \kappa\frac{d\mathcal{E}}{dy} - \rho\gamma A\frac{d\mathcal{E}}{dy}\frac{du}{dy} = \gamma\rho_o v\mathcal{E}_o \end{aligned} \quad (15)$$

or

$$\gamma\mathcal{E} + \frac{1}{2}(u-v)^2 - \frac{\mu}{\rho_o}\left(\frac{v-u}{v}\right)\frac{du}{dy} + A\left(\frac{du}{dy}\right)^2 + \frac{\kappa}{\rho_o v}\frac{d\mathcal{E}}{dy} - \frac{A\gamma}{v-u}\frac{du}{dy}\frac{d\mathcal{E}}{dy} = \gamma\mathcal{E}_o + \frac{1}{2}v^2 \quad (16)$$

From the momentum equation (14), we have

$$\gamma\mathcal{E} = \frac{\gamma}{\gamma-1}(u)(v-u) + \frac{\gamma}{\gamma-1}\frac{\mu}{\rho_o}\left(\frac{v-u}{v}\right)\frac{du}{dy} - \frac{\gamma}{\gamma-1}A\left(\frac{du}{dy}\right)^2 + \gamma\mathcal{E}_o\frac{v-u}{v} \quad (17)$$

Equations (16) and (17) are still exact and independent.

To proceed, we will make the assumption that $\mu = \gamma\kappa$. This is the equivalent to the assumption made in the original discussion of Becker [2] that the Prandtl number of the fluid is 3/4; see also [29] and [25]. That is an excellent approximation for many gases as discussed in [18].

Under that assumption, we note that eq. (16) can be re-written as

$$\Phi + \left[\frac{\mu}{\rho_o v}\frac{du}{dy} - \frac{A}{(v-u)}\left(\frac{du}{dy}\right)^2 \right] \frac{d\Phi}{du} = \Phi_o \quad (18)$$

where Φ is the specific enthalpy:

$$\Phi \equiv \gamma\mathcal{E} + \frac{1}{2}(v-u)^2.$$

Also, eq. (17) can be re-written as

$$\left[\frac{\mu}{\rho_o v}\frac{du}{dy} - \frac{A}{(v-u)}\left(\frac{du}{dy}\right)^2 \right] = \frac{\gamma-1}{(v-u)} \left[\mathcal{E} - \mathcal{E}_o\frac{(v-u)}{v} - \frac{u(v-u)}{(\gamma-1)} \right] \quad (19)$$

Substituting eq. (19) into eq. (18) yields

$$\Phi + \frac{\gamma-1}{(v-u)} \left[\mathcal{E} - \mathcal{E}_o\frac{(v-u)}{v} - \frac{u(v-u)}{(\gamma-1)} \right] \frac{d\Phi}{du} = \Phi_o \quad (20)$$

or

$$\mathcal{E} + \frac{1}{2}(v-u)^2 + \frac{\gamma-1}{(v-u)} \left[\mathcal{E} - \mathcal{E}_o\frac{(v-u)}{v} - \frac{u(v-u)}{(\gamma-1)} \right] \left[\frac{d\mathcal{E}}{du} - (v-u) \right] = \mathcal{E}_o + \frac{1}{2}v^2 \quad (21)$$

This is an ODE for the energy. Observing that both the equation and its boundary conditions are independent of A , the solution will also be independent of A . In particular, the solution for the case $A = 0$, i.e., the Navier–Stokes profile, is well known, namely that Φ is a constant through the shock profile [29, 25]:

$$\mathcal{E} = \mathcal{E}_o + \frac{uv}{\gamma} - \frac{u^2}{2\gamma}. \quad (22)$$

Now, consider that the left-hand-side of eq. (19) vanishes at $u = 0$ and at $u = u_p$. Then the right-hand-side must also vanish for these end points, so that

$$\left[\mathcal{E} - \mathcal{E}_o \frac{(v-u)}{v} - \frac{u(v-u)}{(\gamma-1)} \right] = \alpha_o u (u_p - u) \quad (23)$$

for some constant α_o .

Using eqs. (11) – (13) to eliminate \mathcal{E}_o and u_p in the relation above leads to

$$\left[-\frac{u^2}{2\gamma} + \frac{uv}{\gamma} + \frac{uv}{\gamma(\gamma-1)\mathcal{M}^2} - \frac{u(v-u)}{(\gamma-1)} \right] = \alpha_o u \left[\frac{2v}{\gamma+1} \left(1 - \frac{1}{\mathcal{M}^2} \right) - u \right]. \quad (24)$$

Comparing terms then yields the value of the constant

$$\alpha_o = -\frac{\gamma+1}{2\gamma(\gamma-1)}.$$

Note that eq. (24) is identical in form with eq. (10) of [15]. Thus the *formal* solutions of our eq. (24) can be obtained by re-scaling those in section 2.3 of [15].

Next we combine eqs. (19) and (23)

$$A \left(\frac{du}{dy} \right)^2 - \frac{\mu}{\rho_o} \left(\frac{v-u}{v} \right) \frac{du}{dy} - \alpha_o u (u_p - u) = 0 \quad (25)$$

where

$$\alpha = -(\gamma-1)\alpha_o = \frac{(\gamma+1)}{2\gamma} \Rightarrow \alpha > 0.$$

Solving the quadratic equation (25) for the velocity gradient yields

$$\frac{du}{dy} = \frac{1}{2vA} \left[\frac{\mu}{\rho_o} (v-u) - \sqrt{\frac{\mu^2}{\rho_o^2} (v-u)^2 + 4\alpha A v^2 u (u_p - u)} \right] \quad (26)$$

where we have chosen the minus sign in front of the square root to correspond to a shock moving to the right. Equation (26) may be conveniently rewritten

$$\frac{du}{dy} = \frac{2\alpha\rho_o v}{\mathcal{B}\mu} \left[(v-u) - \sqrt{(v-u)^2 + \mathcal{B}u(u_p - u)} \right] \quad (27)$$

where the parameter

$$\mathcal{B} \equiv \frac{4\alpha A \rho_o^2 v^2}{\mu^2} \quad (28)$$

is dimensionless. Note that \mathcal{B} is related to the critical length scale l_c defined in eq. (28) of [15].

Both Schmidt [37] and Alsmeyer [1] estimate the mean free path²

$$\lambda \approx \frac{16}{5} \left(\frac{\gamma}{2\pi} \right)^{\frac{1}{2}} \frac{\mu}{\rho c}. \quad (29)$$

Most of their data, and all that is used in this paper, is for argon, so that $\gamma = 5/3$ and the constant $\alpha = 0.8$. Then we have the mean free path in the fluid ahead of the shock

$$\lambda_o \equiv 1.65 \frac{\mu \mathcal{M}}{\rho_o v} \quad ; \quad \mathcal{M} = v/c_o \quad (30)$$

and we can nondimensionalize length in the slope equations setting $z \equiv y/\lambda_o$ as is done in the plots of Schmidt and Alsmeyer. In general, then

$$\frac{du}{dz} = \frac{2.64\mathcal{M}}{\mathcal{B}} \left[(v-u) - \sqrt{(v-u)^2 + \mathcal{B}u(u_p-u)} \right] \quad (31)$$

Here, \mathcal{B} is the missing parameter mentioned in the introduction. Using eq. (29) we can rewrite eq. (28) as

$$\mathcal{B} = 8.71\mathcal{M}^2 (A/\lambda_o^2). \quad (32)$$

That is, the parameter \mathcal{B} contains the square of a ratio of length scales – recall the definition of A in eq. (6). In the next section, we will estimate \mathcal{B} from the graphed data of Schmidt and will speculate on the meaning of this parameter. Note that the limit $\mathcal{B} \rightarrow 0$, is perfectly well defined and recovers the Navier–Stokes velocity gradient,

$$\left(\frac{du}{dz} \right)_{NS} = -1.32\mathcal{M} \frac{u(u_p-u)}{(v-u)}. \quad (33)$$

It is possible to solve eq. (31) exactly, in the form $z = Z(u)$ using standard integrals. The results however are complex and we have found it simpler to integrate the ODE numerically to derive $u(z)$. From that discrete solution, it is easy to derive ρ using eq. (7),

$$\rho(z) = \frac{\rho_o v}{(v-u(z))}.$$

Both Schmidt [37] and Alsmeyer [1] estimate the shock width from the measured density profile

$$\mathcal{W} \equiv \rho_{\mathcal{I}} / \left(\frac{d\rho}{dy} \right)_{\mathcal{I}} \quad (34)$$

²See also the footnote on page 676 of [29].

where the subscript \mathcal{I} indicates evaluation at the inflection point where the density gradient is largest in magnitude. Using chain rule

$$\frac{d\rho}{dy} = \frac{d\rho}{du} \frac{du}{dy} = \frac{\rho}{(v-u)} \frac{du}{dy}.$$

Then the shock width is

$$\mathcal{W} = (v - u_{\mathcal{I}}) / \left(\frac{du}{dy} \right)_{\mathcal{I}}. \quad (35)$$

where the subscript still indicates evaluation at the inflection point of the density profile. Note that this differs from a shock width that could be estimated at the inflection point of the velocity profile.

5. Finite Scale Shock Widths

Figure 10 of Schmidt [37] exemplifies much of the discussion in our section 2 as regards shock width. The graph shows three curves that each represent the *inverse* of the shock width as a function of Mach number. The widths are nondimensionalized by the mean free path λ ahead of the shock; mean free path is defined in eq. (29). Curve 1 in the figure shows the theoretical results of Navier–Stokes theory with temperature dependent transport coefficients. Curve 3 shows the theoretical results of Mott Smith theory [30], which Schmidt suggests as a useful, if not totally accurate fit to the data. Clusters of data points at Mach 3,4,6 and 8 illustrate the reproducibility and the scatter of the experimental data. Curve 2 is a solution of the shock profile based on an approximation of the Boltzmann equation. Somewhat hidden in the cluster of data at Mach 8 is a single point calculated using the Discrete Simulation Monte Carlo (DSMC) method of Bird [4, 3] to approximate the solution to the Boltzmann equation. In 1967, this was a heroic calculation using $\approx 10^3$ particles. Recently, DSMC calculations using $\approx 10^{11}$ particles have been reported [9].

To estimate the parameter \mathcal{B} , we will use one piece of information from Figure 10. Because the individual points depend on the temperature dependence of the transport coefficients, which is neglected in our theory, we have chosen to use the *ratio* of the slope widths for one Mach number in the hope that this dimensionless number will be less sensitive to the effects of temperature dependence. In particular, we have chosen to use the values of curve 1 and curve 3 at Mach 4; we selected Mach 4 because curve 3 is nearly flat at this point and also best represents the measured data. We extracted that data directly from the published graph using a web-based data analyzer. The resulting ratio, as well as the analogous ratios at all Mach numbers between 3 and 8 are presented in Table 1.

The agreement of the ratio of shock widths for Mach 4 in the table then is ensured by the choice $\mathcal{B} = 11.1$. Using this value, it is possible to predict the ratios of shock widths for other values of the Mach number. Those values did not contribute to our estimation of \mathcal{B} ; agreement of those calculated values with

<i>Mach No.</i>	<i>MS</i>	<i>NS</i>	<i>ratio</i>	<i>calc.</i>
3	0.283	0.446	1.58	1.60
4	0.305	0.521	1.71	1.71
5	0.304	0.539	1.77	1.77
6	0.294	0.536	1.82	1.81
7	0.283	0.524	1.85	1.84
8	0.273	0.510	1.87	1.85

Table 1: Captured data from Figure 10 of [37]. The column labeled *MS* is from curve 3, and the column labeled *NS* is from curve 1. The columns labeled *MS* and *NS* represent the inverse of shock widths from Mott-Smith theory and Navier-Stokes theory. The ratio of those widths and analogous ratios computed from finite scale theory are compared in Fig. 1.

the estimates taken from Figure 10 validate our hypothesis that \mathcal{B} is a constant independent of Mach number and is a first step in validating the use of a finite scale model to predict shock structure. A plot of the results in Table 1 is shown in Figure 1.

Combining eq. (32) and eq. (6)

$$A = 1.34\lambda_o^2/\mathcal{M}^2 \equiv \frac{1}{3} \left(\frac{\Delta x}{2} \right)^2$$

so that we estimate

$$\Delta x \approx 0.96\lambda_o \tag{36}$$

for the Mach 4 shock. Qualitatively then, our result that \mathcal{B} is a constant for a wide range of Mach numbers implies that the averaging scale Δx is in fact proportional to the mean free path, which is the only fundamental length scale of kinetic theory. However, we can extend the analysis more quantitatively as follows.

We have measured the shock width in terms of the mean free path in the quiescent fluid ahead of the shock so as to be consistent with the reported data of Schmidt [37] and Alsmeyer [1]. However as implied by eq. (29), the mean free path at the inflection point of the density profile will be smaller as both the sound speed and the density grow larger as the shock passes. Estimating the mean free path at the inflection point, where fluid velocity is $u_{\mathcal{I}}$,

$$\lambda_{\mathcal{I}} = 1.65 \frac{\mu}{\rho_{\mathcal{I}} c_{\mathcal{I}}} = \lambda_o \left(\frac{\rho_o c_o}{\rho_{\mathcal{I}} c_{\mathcal{I}}} \right)$$

Data from numerical integration to calculate the ratio $\left(\frac{\rho_o c_o}{\rho_{\mathcal{I}} c_{\mathcal{I}}} \right)$ is presented in Table 2. A plot of that ratio vs. the inverse of the Mach number is shown in

$Mach$	$\rho_{\mathcal{I}}/\rho_o$	$u_{\mathcal{I}}/v$	$\lambda_{\mathcal{I}}/\lambda_o$
3	2.28	1.68	0.403
4	2.54	2.43	0.268
5	2.69	3.14	0.187
6	2.77	3.84	0.136
7	2.85	4.54	0.104
8	2.86	5.2	0.080

Table 2: Showing the ratio of the mean free path measured at the inflection point of density to the mean free path measured in the undisturbed fluid ahead of the shock as a function of Mach number. Data is plotted in Fig. 2.

Fig. 2, indicating a nearly perfect linear relation

$$\lambda_{\mathcal{I}}/\lambda_o \approx 1.56/M. \quad (37)$$

Then, inserting eq. (37) into eq. (32),

$$\mathcal{B} = 1.77 \left(\frac{\Delta x}{\lambda_{\mathcal{I}}} \right)^2. \quad (38)$$

That is, when shock width is measured in terms of the number of mean free paths at the inflection point of density, the parameter \mathcal{B} is a universal constant not dependent on Mach number. Finally, invoking our estimate $\mathcal{B} = 11.1$, we find

$$\Delta x \approx 2.57\lambda_{\mathcal{I}} \quad (39)$$

for all Mach numbers between 3 and 8. Perhaps fortuitously, that estimate is consistent with Lagrangian shock-capturing algorithms where an artificial viscosity chosen to yield a shock width of about 3 computational cells suffices to eliminate unphysical post-shock oscillations; see [47] and the discussion in section 7 of [25].

6. Comparisons and Trends

Here we compare some aspects of the finite scale versus the Navier–Stokes solutions, and show trends of the finite scale solutions as a function of shock strength (Mach number). The “data” in Figures 3 through 7 were all generated by numerical integration of the ODEs – equation (31) for finite scale and (33) for Navier–Stokes. We remind that neither of those equations incorporate the effects of temperature dependence of the transport coefficients, which would make the derivation of the traveling wave ODEs very difficult. On the other

hand, full solution of the PDEs with temperature dependence is very feasible on the computer. We will return to this point in section 7.

In the rest of this section, we will abbreviate Navier–Stokes as NS to avoid lengthy repetitions. To begin, we offer some structural observations. Consider Fig. 4 comparing the velocity profiles of the NS solution to that of the FS solution for a Mach 4 shock. We have arbitrarily chosen the center of the shock, where $u = \frac{1}{2}u_p$ at $z = 0$ for both profiles. The enveloping theorem proven in the appendix states that the FS profile will lie underneath the NS profile on the upstream side of the intersection point (to the left in the figure) and will lie above the NS curve to the right (downstream) side of the NS profile. Since the NS profile does not have compact support, the theorem shows that the FS profile also cannot have compact support.

That result is not surprising, but is a direct result of including physical viscosity. We note that the analysis of the adiabatic FS in [28] also only achieves compact support in the limit of vanishing physical viscosity. The lack of compact support is also a principal consideration leading to the local definition (i.e., at the inflection point of density) of shock width in eq. (35) as opposed to using a more global and possibly subjective metric.

The lack of compact support implies that the velocity profile is monotone. If there were a local maximum (or minimum) within the profile, the slope would vanish which means that either $u = u_p$ or $u = 0$. Then a piecewise continuous compact solution could be formulated contradicting the enveloping theorem. Further, applying the chain rule shows that the monotonicity of velocity implies the monotonicity of the density and internal energy. Using eq. (7)

$$\frac{d\rho}{dz} = \frac{d\rho}{du} \frac{du}{dz} = \frac{\rho_o v}{(v-u)^2} \frac{du}{dz}. \quad (40)$$

Similarly, using eq. (22),

$$\frac{d\mathcal{I}}{dz} = \frac{d\mathcal{I}}{du} \frac{du}{dz} = \frac{(v-u)}{\gamma} \frac{du}{dz}. \quad (41)$$

These monotonicity results are confirmed graphically in Figs. 3 and 6.

In Fig. 3 we compare the NS and FS density profiles for the Mach 4 shock. One might conclude from this figure that the front of the NS profile is close to that of the FS profile and that the bigger differences occur near the back of the shock. However, this is illusory. If we had chosen to center the two density profiles say at a value of $\rho/\rho_o = 2$ instead of at $\rho/\rho_o = 1.5$, the differences would look more symmetric about $z = 0$. Despite this ambiguity, the slope at the inflection point and hence the shock width are both independent of the choice of centering.

A better way to assess symmetry of the density profiles is to use the normalized density profile

$$R \equiv \frac{\rho - \rho_o}{\rho_{max} - \rho_o} \quad (42)$$

where ρ_{max} is the final density at the back of the shock. The R function comparison of normalized density allows for direct comparison of shocks with different

Mach numbers. Fig. 5 compares the normalized density profiles for FS shocks of Mach 4 and Mach 8.

In [29], Morduchow and Libby also calculated the equilibrium entropy profile in the NS shock. Their result showed that the entropy is not monotone inside the shock, but has a peak. This surprising result has been discussed often in the literature and has been found not to violate the second law of thermodynamics in the sense of the Clausius–Duhem inequality [25]. In Fig. 7, we calculate the FS entropy for the Mach 4 shock. That profile has a broader peak than the NS entropy although its peak value and position in the profile are very similar. For the sake of completeness, we add that the inside of a shock is very far from equilibrium [25].

7. Summary and Discussion

The subject of this paper is the structure of shocks in perfect gases and our goal is to demonstrate the ability of a continuum model based on finite scale theory to accurately reproduce that structure, which has been precisely measured in many laboratory experiments. We began by documenting the history and failure of Navier–Stokes theory to describe the measured shock profiles. We then provided a brief description of finite scale theory and motivation for why it might provide a more accurate prediction of shock structure. That motivation focused mainly on the property of anomalous dissipation, which would engender broader shock structure more in accord with the experimental measurements.

In our first principal result, we constructed a traveling wave formulation of the full finite scale equations, including physical viscosity and heat conduction, and the additional finite scale fluxes of momentum and energy; cf. eq. (31). That analysis identified a key continuum scale parameter, \mathcal{B} , cf. eq. (28). In our second principal result, we used the traveling wave solution to expose the relation between \mathcal{B} and the microscale (kinetic) parameter λ , the molecular mean free path. We illustrated how \mathcal{B} could be roughly estimated from published experimental data and demonstrated the universality of that parameter.

In our third principal result, we explored some of the properties of the finite scale solution. We proved those solutions are not compact, and that the predicted profiles of velocity, density and internal energy are monotone. We also exhibited numerical solutions of the equations to compare with Navier–Stokes theory and to graphically verify the theoretical results.

In the introduction, we acknowledged that this paper represents only the first step toward our goal of validating a finite scale model of shock structure. We identified two important missing elements. First, our model lacks at least one physical effect that strongly influences shock shape, namely the dependence of physical viscosity and heat conductivity on the temperature. Second, we have offered no theory for calculating the parameter \mathcal{B} , even though the determination from experimental data has proven successful. Nevertheless, we believe that our results so far indicate that finite scale theory offers a promising alternative for predicting shock wave structure in perfect gases.

Becker's 1922 analysis [2] of Navier–Stokes theory applied to the shock structure of perfect gases also neglected the temperature dependence of the coefficients of heat conduction and of viscosity. Thomas [42] noted that these coefficients would increase as temperature increased. It was the main purpose of the 1949 paper of Morduchow & Libby [29] to quantify the importance of that dependence. Indeed, temperature dependence did broaden the predicted shocks, though not enough to mollify Becker's criticism. Computer simulation was barely nascent in 1949, but now it is feasible to perform fully resolved simulations of shock propagation in three spatial dimensions using finite volume methods. That numerical capability was demonstrated in [25] for Navier–Stokes theory where the accuracy of simulation was verified by comparison with analytic solutions. A version of that computer program is now capable of simulating the finite scale equations with temperature dependent transport coefficients [34].

We speculate that the magnitude of the parameter \mathcal{B} – i.e., how many mean free paths are represented in the finite length scale; see eq. (39) – is related to the breakdown of the continuum approximation. The connection of \mathcal{B} to the mean free path results primarily from dimensional analysis and from the older connection of physical viscosity to the mean free path exposed by the Chapman–Enskog approximation [6, 17]. An extension of the Chapman–Enskog approximation that begins with the Boltzmann equation and leads to the finite scale equations has recently been published [22] and may provide a starting point for additional theory.

A central presence in this paper has been the concept of anomalous dissipation. This idea is originally found in the theoretical work of Onsager [7] and Kolmogorov [8] where it appears somewhat amorphously. On the other hand, the subject of regularizing the Euler equations [24] and the definitive form of artificial viscosity [46] have been of fundamental importance to the numerical community since the beginning of computational fluid dynamics. The recognition of the congruence of these two ideas owes much to the intuition of early pioneers of ILES [11].

APPENDIX – An Enveloping Theorem

Observing the comparison of profiles, Navier–stokes (NS) vs. finite scale (FS), in Figs. 3 and 4 two properties seem clear,

- the profiles intersect only once.
- upstream of the intersection, the FS profile always lies beneath the NS profile, while downstream of the intersection the FS profile always lies above the NS profile. We will term this an *enveloping property*.

In this appendix, we prove those observations. The proof is complicated by the lack of explicit solutions, i.e., velocity as a function of coordinate and by the autonomous nature of the ODEs.

Since the traveling wave problem is formulated with boundary conditions at $-\infty$ and $+\infty$, it is necessary to specify velocity at one point in the solution.

This can be done arbitrarily and in our numerical simulations, we have chosen to specify the center of the profile, such that $u = u_p/2$ at $z = 0$. As all of our plots and equations represent shocks moving to the right, we will refer to regions left of the intersection point as upstream and right of the intersection point as downstream.

Theorem: consider the solutions to the ODEs of eq. (33) representing NS and of eq. (31) representing FS. These solutions have only one intersection point. Further, the NS solution envelopes the FS solution.

Proof: The enveloping property implies that the upstream NS velocity should be larger than the upstream FS velocity for the same value of coordinate z . Fig. 8 shows the same NS and FS velocity profiles as reported in Fig. 4, but rotated 90° counterclockwise. Then it is clear that the enveloping property can also be formulated to say that the NS solution will have larger coordinate than the FS solution for *same value of velocity*. This is a more useful formulation since the coordinate difference can be written down formally.

First, we rewrite the ODE (31)

$$\frac{du}{dz} = C \frac{u(u_p - u)}{(v - u) + \sqrt{(v - u)^2 + \mathcal{B}u(u_p - u)}} \quad (43)$$

where $C = 2.58\mathcal{M}$. Then a formal solution for the FS coordinate at velocity u_* is

$$\int_{\frac{u_p}{2}}^{u_*} \frac{du}{u(u_p - u)} \left[(v - u) + \sqrt{(v - u)^2 + \mathcal{B}u(u_p - u)} \right] = C \int_0^{z_{FS}} dz. \equiv Cz_{FS} \quad (44)$$

Similarly, a formal solution for the NS coordinate can be written:

$$\int_{\frac{u_p}{2}}^{u_*} \frac{du}{2u(u_p - u)} (v - u) = C \int_0^{z_{NS}} dz \equiv Cz_{NS} \quad (45)$$

Combining these equations,

$$C\Delta z \equiv C(z_{NS} - z_{FS}) = \int_{\frac{u_p}{2}}^{u_*} du (v - u) \chi \left[\frac{1}{2} - \frac{1}{1 + \sqrt{1 + \mathcal{B}\chi}} \right] \quad (46)$$

where

$$\chi = \frac{u(u_p - u)}{(v - u)^2} > 0 \quad ; \quad u \in (0, u_p).$$

Also,

$$\left[\frac{1}{2} - \frac{1}{1 + \sqrt{1 + \mathcal{B}\chi}} \right] > 0 \quad ; \quad \mathcal{B} > 0.$$

and

$$v - u > 0$$

So then the integrand is always positive and we conclude

$$\Delta z > 0 \quad \text{if } u_* > \frac{u_p}{2}, \quad (47)$$

$$\Delta z < 0 \quad \text{if } u_* < \frac{u_p}{2}. \quad (48)$$

Note that the proof holds generally for all Mach numbers, all values of $\mathcal{B} > 0$ and any realizable value of the common velocity that appears at the intersection point.

DEDICATION

For David from Len: Remembering more than 40 years of science and friendship, hiking and cross-Atlantic flights.

ACKNOWLEDGMENTS

We gratefully acknowledge many illuminating discussions with M. Gallis, P.M. Jordan and D.E. Vaughan. This work was performed under the auspices of the U.S. Department of Energy's NNSA by the Los Alamos National Laboratory, is managed by Triad National Security, LLC for the National Nuclear Security Administration of the U.S. Department of Energy under contract 89233218CNA000001.

- [1] H. Alsmeyer, 1976: "Density profiles in argon and nitrogen shock waves measured by the absorption of an electron beam," *J. Fluid Mech.* **74**, 497–513.
- [2] R. Becker, 1922: "Stoßwelle und detonation," (In German), *Zeitschrift für Physik* **8** 321–362.
- [3] G.A. Bird, 1967: "The velocity distribution function within a shock wave," *J. Fluid Mech.* **30**, 479–487.
- [4] G.A. Bird, **Molecular Gas Dynamics and the Direct Simulation of Gas Flows**, Oxford Engineering Science Series, 2nd edition, Clarendon Press, Oxford, UK, (1994).
- [5] C. Cai, D.D. Liu & K. Xu, 2008: "One-dimensional multiple-temperature gas-kinetic Bhatnagar-Gross-Kook scheme for shock wave computation," *AIAA Journal* **46**, 1054–1062.
- [6] S. Chapman & T.G. Cowling, **The Mathematical Theory of Non-uniform gases**, Cambridge University Press, Cambridge, UK, 3rd ed. (1970).
- [7] G.L. Eyink & K.R. Sreenivasan, 2006: "Onsager and the theory of hydrodynamic turbulence," *Rev. Mod. Physics* **78**, 87–135.

- [8] U. Frisch, **Turbulence, The Legacy of A. N. Kolmogorov**, Cambridge University Press, Cambridge, 1995.
- [9] M.A. Gallis, T.P. Koehler, J.R. Torczynski & S.J. Plimpton, 2015: “Direct simulation Monte Carlo investigation of the Richtmyer–Meshkov instability,” *Phys. Fluids* **27**, 084105.
- [10] L.S. García-Colín, R.M. Velasco & F.J. Uribe, 2008: “Beyond the Navier–Stokes equations: Burnett hydrodynamics,” *Phys. Reports* **465**, 149–189.
- [11] F.F. Grinstein, L.G. Margolin & W.J. Rider, **Implicit Large Eddy Simulation: Computing Turbulent Fluid Dynamics**, Cambridge University Press, Cambridge, UK, 2007.
- [12] C.W. Hirt, 1968: “Heuristic stability theory for finite difference equations. *J. Comput. Phys.* **2**, 339–355.
- [13] B.L. Holian, 1988: “Modeling shock-wave deformation via molecular dynamics,” *Phys. Rev. A*, 2562–2568.
- [14] B.L. Holian, M. Mareschal & R. Ravelo, 2011: “Burnett–Cattaneo continuum theory for shock waves,” *Phys. Rev. E***83**, 026703.
- [15] P.M. Jordan & R.S. Keiffer, 2015: “A note on finite-scale Navier–Stokes theory: The case of constant viscosity, strictly adiabatic flow,” *Phys. Lett. A***379**, 124–130.
- [16] I.W. Kokkinakis, D. Drikakis & D.L. Youngs, 2019: “Modeling of Rayleigh–Taylor mixing using single-fluid models,” *Phys. Rev. E***99**, 013104.
- [17] G.M. Kremer, **An Introduction to the Boltzmann Equation and Transport Processes in Gases**. New York: Springer (2010).
- [18] H.W. Liepmann, R. Narasimha & M.T. Chahine, 1962: “Structure of a plane shock layer,” *Phys. Fluids* **5**, 371–377.
- [19] P.F. Linden, J.M. Redondo & D.L. Youngs: “Molecular mixing in Rayleigh–Taylor instability,” *J. Fluid Mech.* **265**, 97–124.
- [20] L.G. Margolin, 2009: “Finite-scale equations for compressible fluid flow,” *Phil. Trans. R. Soc. A* **367**, 2861–2871.
- [21] L.G. Margolin, 2014: “Finite scale theory: the role of the observer in classical fluid flow,” *Mech. Res. Comm.* **57**, 10–17.
- [22] L.G. Margolin, 2018: “Scale matters,” *Phil. Trans. R. Soc. A***376**:20170235.
- [23] L.G. Margolin & R.S. Baty, 2019: “Conservation laws in discrete geometry,” *J. Geom. Mech.* **11**, 187–203.
- [24] L.G. Margolin & C.S. Plesko, 2019: “Discrete regularization,” *Evolution Equations and Control Theory* **8**, 117–137.

- [25] L.G. Margolin, J.M. Reisner & P.M. Jordan, 2017: “Entropy in self-similar shock profiles,” *Int. J. Nonlinear Mech.* **95**, 333–346.
- [26] L.G. Margolin & W.J. Rider, 2002: “A rationale for implicit turbulence modeling,” *Int. J. Num. Meth. Fluids* **39**, 821–841.
- [27] L.G. Margolin & P.K. Smolarkiewicz, 1999: “Large-eddy simulations of convective boundary layers using nonoscillatory differencing,” *Physica D* **133**, 390–397.
- [28] L.G. Margolin & D.E. Vaughan, 2012: “Traveling wave solutions for finite scale equations,” *Mech. Res. Comm.* **45**, 64–69.
- [29] M. Morduchow & P.A. Libby, 1949: “On a complete solution of the one-dimensional flow equations of a viscous, heat-conducting, compressible gas,” *J. Aeronautical Sciences* **16**, 674–684, and 704.
- [30] H. M. Mott-Smith, 1951: “The solution of the Boltzmann equation for a shock wave,” *Phys. Rev.* **82**, 885–892.
- [31] E.S. Oran & J.P. Boris, 1993: “Computing turbulent shear flows – a convenient conspiracy,” *Computers in Physics* **7**, 523–533.
- [32] D.H. Porter, A. Pouquet & P.R. Woodward, 1998: “Kolmogorov-like spectra in decaying three-dimensional supersonic flows,” *Phys. Fluids* **6**, 2133–2142.
- [33] Lord Rayleigh, Aerial plane waves of finite amplitude, *Proc. R. Soc. Lond. Ser. A* **84** (1910) 247–284.
- [34] J. Reisner, J. Serencsa & S. Shkoller, 2013: “A space-time smooth artificial viscosity method for nonlinear conservation laws,” *J. Comput. Phys.* **235**, 912–933.
- [35] M.H. Saadat, F. Bösch & I.V. Karlin, 2019: “Lattice Boltzmann model for compressible flows on standard lattices: Variable Prandtl number and adiabatic exponent,” *Phys. Rev. E*, 013306.
- [36] M.D. Salas, 2007: “The curious events leading to the theory of shock waves,” *Shock Waves* **16**, 477–487.
- [37] B. Schmidt, 1969: “Electron beam density measurements in shock waves in argon,” *J. Fluid Mech.* **39**, 361–373.
- [38] J. Smagorinsky, “Some historical remarks on the use of nonlinear viscosities,” in **Large Eddy Simulation of Complex Engineering and Geophysical Flows**, B. Galperin & S. A. Orszag, eds., Cambridge University Press, Cambridge, UK (1993), 3–36.
- [39] C. Sun, 2000: “Simulations of compressible flows with strong shocks by an adaptive lattice Boltzmann model,” *J. Comput. Phys.* **161**, 70–84.

- [40] G.I. Taylor, 1910: “The conditions necessary for discontinuous motion in gases,” Proc. R. Soc. Lond. Ser. A 84, 371–377.
- [41] H. Tennekes & J.L. Lumley, **A First Course in Turbulence**, MIT press, Cambridge MA (1972).
- [42] L.H. Thomas, 1944: “Note on Becker’s theory of the shock front,” J. Chem. Phys. **12**, 449–453.
- [43] B. Thornber, D. Drikakis, D.L. Young & R.J.R. Williams, 2010: “The influence of initial conditions on turbulent mixing due to Richtmyer–Meshkov instability,” J. Fluid Mech. **654**, 99–139.
- [44] F.J. Uribe, “The shock wave problem revisited: the Navier–Stokes equations and Brenner’s two velocity hydrodynamics,” in: A.N. Gorban, D. Roose (Eds.), *Coping with Complexity: Model Reduction and Data Analysis*, Springer, 2011, pp. 207–233.
- [45] B. van Leer, 1977: “Towards the ultimate conservative difference scheme. Part IV. A new approach to numerical convection,” J. Comput. Phys. **23**, 276–299.
- [46] J. von Neumann & R.D. Richtmyer, 1950: “A method for the numerical calculation of hydrodynamic shocks,” J. Appl. Phys. **21**, 232–237.
- [47] M.L. Wilkins, 1980: “Use of artificial viscosity in multidimensional fluid dynamic calculations,” J. Comput. Phys. **36**, 281–303.
- [48] D.L. Youngs, 1984: “Numerical simulation of turbulent mixing by Rayleigh–Taylor instability,” Physica **12D**, 32–44.
- [49] D.L. Youngs, 1991: “Three-dimensional numerical simulation of turbulent mixing by Rayleigh–Taylor instability,” Phys. Fluids **A3**, 1312–1320.
- [50] D.L. Youngs, 1994: “Numerical simulation of mixing by Rayleigh–Taylor and Richtmyer–Meshkov instability,” Laser Part. Beams **12**, 725–750.
- [51] D.L. Youngs, 2003: “Application of MILES to Rayleigh–Taylor and Richtmyer–Meshkov mixing,” Paper 2003-4102, AIAA.
- [52] D.L. Youngs, 2013: “The density ratio dependence of self-similar Rayleigh–Taylor mixing,” Phil. Trans. R Soc **371**, 20120173.
- [53] Y. Zhou, 2017: “Rayleigh–Taylor and Richtmyer–Meshkov instability induced flow, turbulence, and mixing. I,” Physics Reports **720–722**, 1–136.
- [54] Y. Zhou, 2017: “Rayleigh–Taylor and Richtmyer–Meshkov instability induced flow, turbulence, and mixing. II,” Physics Reports **723–725**, 1–160.

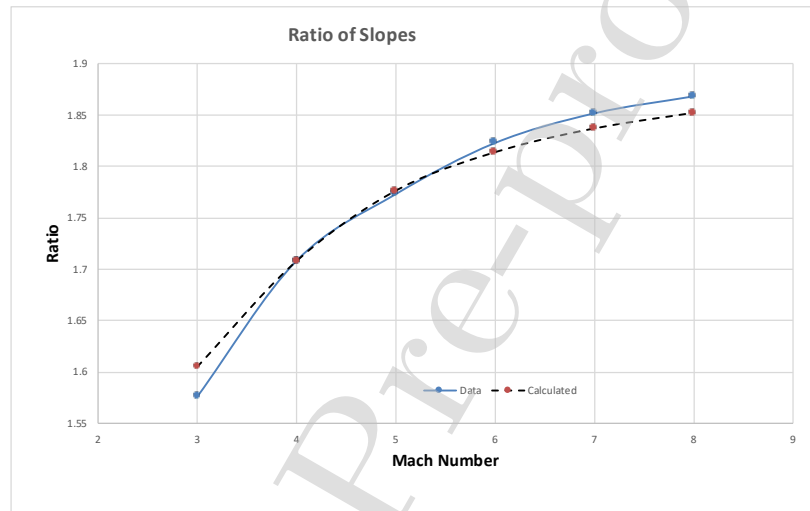


Figure 1: Points on this graph represent a ratio of slopes of the shock profile, as defined in eq. (35). The solid curve values are calculated from values extracted from Figure 10 in [37] and reproduced in Table 1. The values in the dotted curve are calculated from eqs. (31) and (33). The parameter \mathcal{B} in the finite scale theory was chosen to ensure the equality at Mach 4. The comparison of points at other Mach numbers is a critical test of the applicability of finite scale theory to model shock structure..

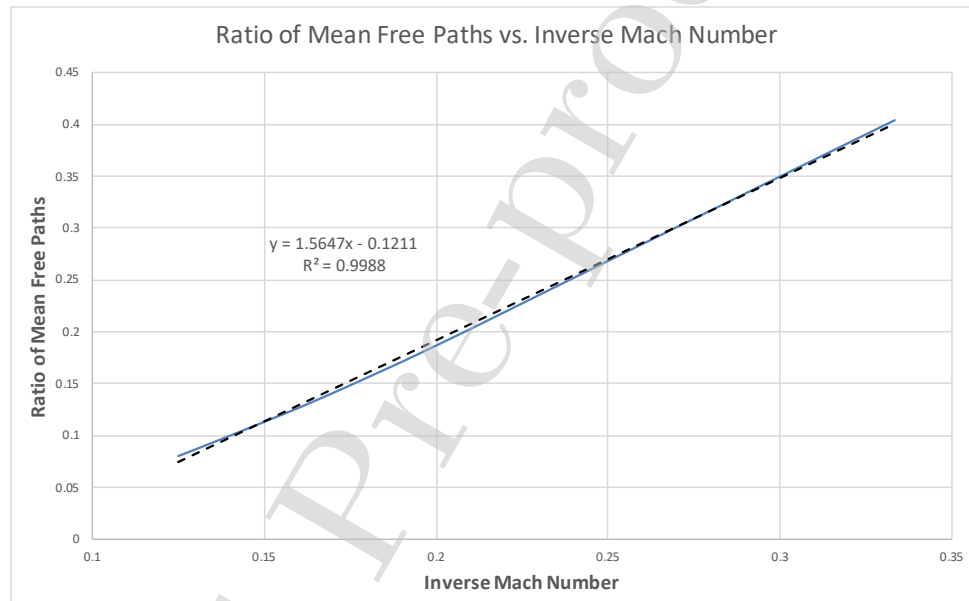


Figure 2: The ratio of mean free paths measured at the inflection point of the density profile and in the undisturbed fluid ahead of the shock is plotted versus the inverse of the Mach number. The plot is linear with a small offset for very strong shocks. Data for this plot is shown in Table 2.

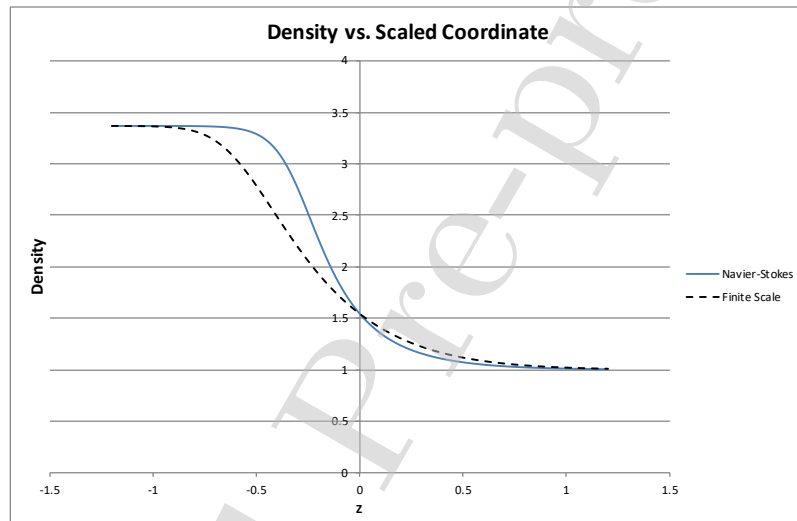


Figure 3: The profiles of normalized density ρ/ρ_0 in a Mach 4 shock as predicted by finite scale theory (dashed curve) and by Navier–Stokes theory (solid curve) are plotted versus a scaled coordinate nondimensionalized by the mean free path in the undisturbed fluid.

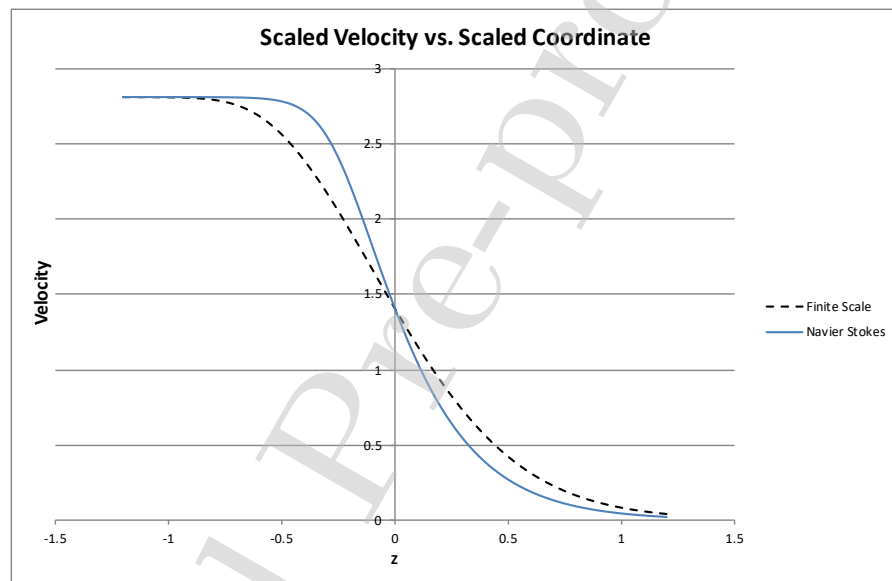


Figure 4: The profiles of normalized velocity u/c_o in a Mach 4 shock as predicted by finite scale theory (dashed curve) and by Navier–Stokes theory (solid curve) are plotted versus a scaled coordinate nondimensionalized by the mean free path in the undisturbed fluid.

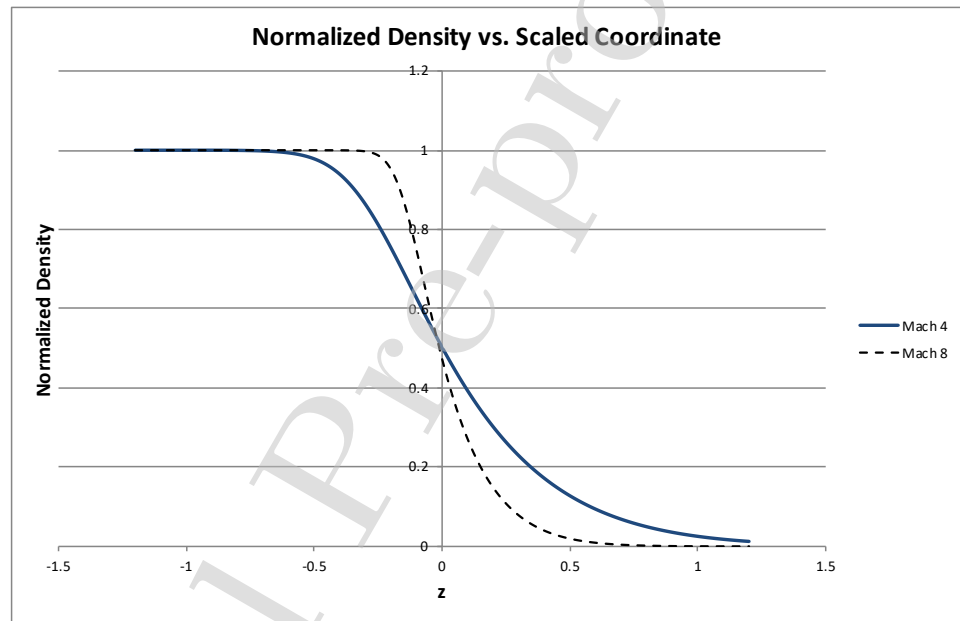


Figure 5: The normalized density $R = (\rho - \rho_o) / (\rho_{max} - \rho_o)$ for the Mach 4 shock (dotted curve) and the Mach 8 shock (solid curve) are plotted versus a scaled coordinate nondimensionalized by the mean free path in the undisturbed fluid.

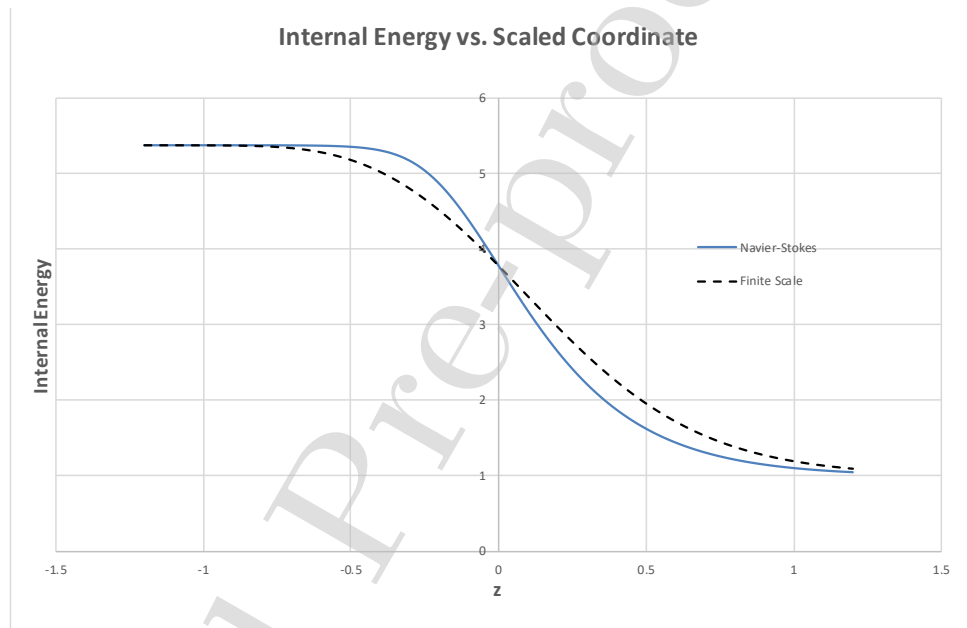


Figure 6: The scaled internal energy $\mathcal{I}/\mathcal{I}_0$ for the Mach 4 shock as predicted by finite scale theory (dashed curve) and by Navier–Stokes theory (solid curve) are plotted versus a scaled coordinate nondimensionalized by the mean free path in the undisturbed fluid.

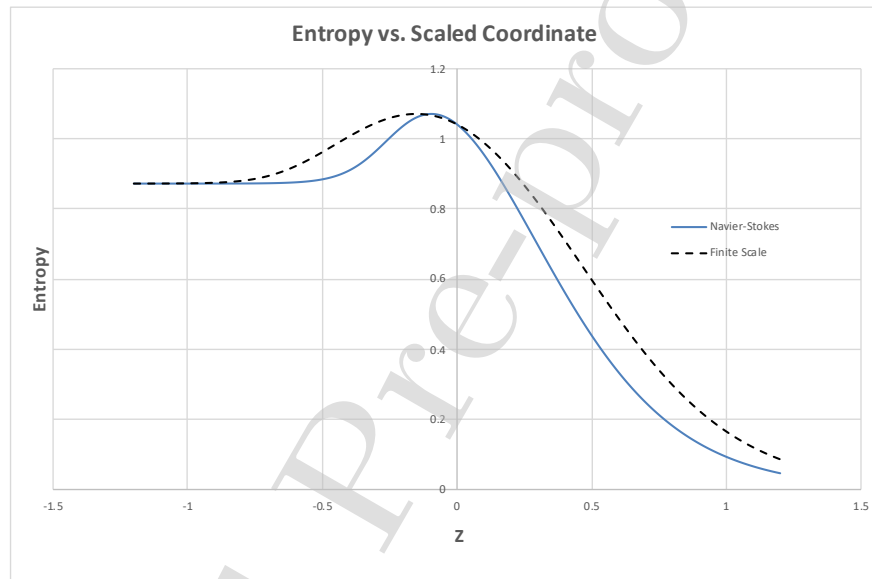


Figure 7: Nondimensional entropy S/c_v as predicted by finite scale theory (dashed curve) and by Navier–Stokes theory (solid curve) are plotted versus a scaled coordinate nondimensionalized by the mean free path in the undisturbed fluid. Note the peaks in both curves.

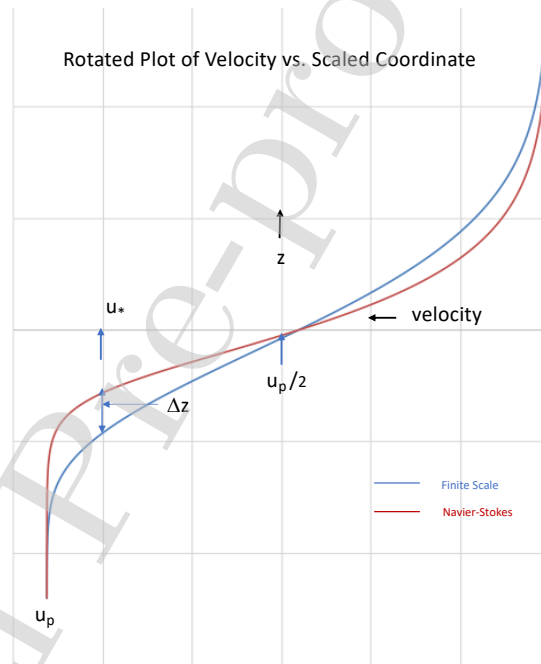


Figure 8: The profiles of normalized velocity u/c_o in a Mach 4 shock as predicted by finite scale theory (dashed curve) and by Navier–Stokes theory (solid curve) are plotted versus a scaled coordinate nondimensionalized by the mean free path in the undisturbed fluid. The profiles are the same as in Fig. 4 but rotated by 90° and with some notation added relevant to the Appendix.

Highlights for

A Finite Scale Model for Shock Structure

L.G. Margolin, C.S. Plesko, J.M. Reisner

- 1) A review of the history of analytic studies of shock structure in a perfect gas.
- 2) A review of finite scale theory.
- 3) Analytic solutions of shock structure for a perfect gas.
- 4) A comparison of predicted and measured shock widths for a perfect gas.

Nov. 4, 2019

We declare no conflict of interest.

Len Margolin

Jon Reisner

Catherine Plesko

Journal Pre-proof